

LGR4 is a receptor for RANKL and negatively regulates osteoclast differentiation and bone resorption

Jian Luo^{1,7}, Zhengfeng Yang^{1,7}, Yu Ma¹, Zhiying Yue¹, Hongyu Lin¹, Guojun Qu¹, Jinping Huang¹, Wentao Dai², Chenghai Li¹, Chunbing Zheng¹, Leqin Xu¹, Huaqing Chen¹, Jiqui Wang³, Dali Li¹, Stefan Siwko⁴, Josef M Penninger⁵, Guang Ning³, Jianru Xiao^{1,6} & Mingyao Liu^{1,4}

Tumor necrosis factor (TNF) superfamily member 11 (TNFSF11, also known as RANKL) regulates multiple physiological or pathological functions, including osteoclast differentiation and osteoporosis. TNFSF11A (also called RANK) is considered to be the sole receptor for RANKL. Herein we report that leucine-rich repeat-containing G-protein-coupled receptor 4 (LGR4, also called GPR48) is another receptor for RANKL. LGR4 competes with RANK to bind RANKL and suppresses canonical RANK signaling during osteoclast differentiation. RANKL binding to LGR4 activates the G_{α_q} and GSK3- β signaling pathway, an action that suppresses the expression and activity of nuclear factor of activated T cells, cytoplasmic, calcineurin-dependent 1 (NFATC1) during osteoclastogenesis. Both whole-body (*Lgr4*^{-/-}) and monocyte conditional knockout mice of *Lgr4* (*Lgr4* CKO) exhibit osteoclast hyperactivation (including elevation of osteoclast number, surface area, and size) and increased bone erosion. The soluble LGR4 extracellular domain (ECD) binds RANKL and inhibits osteoclast differentiation *in vivo*. Moreover, LGR4-ECD therapeutically abrogated RANKL-induced bone loss in three mouse models of osteoporosis. Therefore, LGR4 acts as a second RANKL receptor that negatively regulates osteoclast differentiation and bone resorption.

Bone-mass regulation depends on the dynamic balance between bone formation and bone resorption, which are driven by osteoblast activation and osteoclast activation, respectively. RANKL is a central positive regulator of osteoclast differentiation, acting through its binding to TNFSF11A to induce signaling through TNF-receptor-associated factor (TRAF) and nuclear factor (NF)- κ B, which ultimately leads to the activation of NFATC1. *Tnfsf11*^{-/-} mice exhibit osteopetrosis as a result of a lack of osteoclasts^{1,2}; defective T cell and B cell differentiation²; and a failure of mammary gland lobuloalveolar development during pregnancy³. RANKL has been implicated in breast carcinogenesis and bone metastasis⁴⁻⁷, diabetes⁸, and body-temperature regulation⁹. The balance between RANKL and its decoy receptor osteoprotegerin (OPG, also called TNFSF11B) is considered to be a crucial determinant of bone resorption¹⁰. Denosumab, a human monoclonal antibody against RANKL, is an approved therapeutic for treating postmenopausal osteoporosis and giant cell tumor of bone¹¹.

LGR4, also known as GPR48, regulates multiple developmental pathways through either potential classical G-protein signaling^{12,13} or via the potentiation of Wnt signaling^{14,15}. A nonsense mutation in *LGR4* is associated with low bone mineral density (BMD) in humans¹⁶. However, the molecular mechanisms for this regulation are unknown. LGR4 belongs to the LGR family, in which another

two members, thyroid-stimulating hormone receptor (TSHR) and follicle-stimulating hormone receptor (FSHR), regulate osteoclast differentiation and resorption^{17,18}. Therefore, we speculated whether LGR4 could also regulate osteoclast differentiation.

Tnfsf11^{-/-} mice and *Lgr4*^{-/-} mice present with similar sets of phenotypes, including disrupted immunity regulation^{2,19}, mammary gland development^{3,20}, body-temperature modulation^{9,21}, cancer metastasis^{4-7,22,23}, and energy expenditure^{8,21}. RANKL-RANK signaling regulates mammary gland lobuloalveolar progenitors, at least in part, through the LGR4 ligand R-spondin1 (RSPO1), which suggests the potential for crosstalk between RANKL-RANK and LGR4 signaling²⁴. Therefore, we hypothesized that RANKL and LGR4 act in the same pathways to regulate physiological functions. In this study, we reveal that LGR4 is another receptor for RANKL, and that it, via this ligand, acts to negatively regulate osteoclast differentiation and bone remodeling. These findings suggest that targeting LGR4 is a viable strategy for treating osteoporosis and other bone-resorption diseases.

RESULTS

LGR4 physically interacts with RANKL

To test our hypothesis that RANKL and LGR4 act in the same pathways, we employed five separate approaches to determine whether

¹East China Normal University and Shanghai Changzheng Hospital Joint Research Center for Orthopedic Oncology, Shanghai Key Laboratory of Regulatory Biology, Institute of Biomedical Sciences and School of Life Sciences, East China Normal University, Shanghai, China. ²Shanghai Center for Bioinformation Technology, Shanghai Academy of Science and Technology, Shanghai, China. ³Department of Endocrinology and Metabolism, Ruijin Hospital, Shanghai Jiao Tong University School of Medicine, Shanghai, China. ⁴Department of Molecular and Cellular Medicine, Institute of Biosciences and Technology, Texas A&M University Health Science Center, Houston, Texas, USA. ⁵IMBA, Institute of Molecular Biotechnology of the Austrian Academy of Sciences, Vienna, Austria. ⁶Department of Orthopedic Oncology, Shanghai Changzheng Hospital, The Second Military Medical University, Shanghai, China. ⁷These authors contributed equally to this work. Correspondence should be addressed to J.L. (jluo@bio.ecnu.edu.cn), J.X. (jianruxiao83@163.com) or M.L. (myliu@bio.ecnu.edu.cn or mliu@ibt.tamhsc.edu).

Received 14 August 2015; accepted 5 March 2016; published online 11 April 2016; doi:10.1038/nm.4076

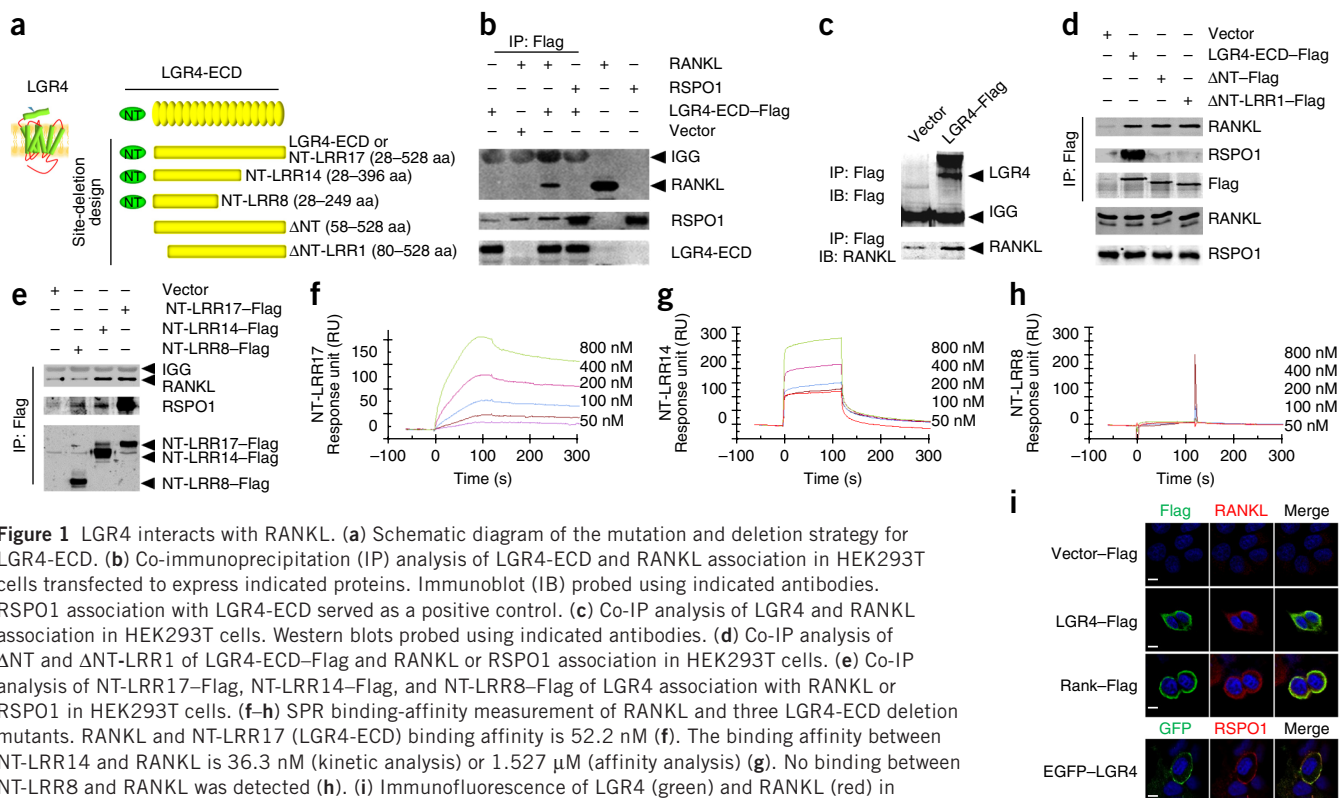


Figure 1 LGR4 interacts with RANKL. (a) Schematic diagram of the mutation and deletion strategy for LGR4-ECD. (b) Co-immunoprecipitation (IP) analysis of LGR4-ECD and RANKL association in HEK293T cells transfected to express indicated proteins. Immunoblot (IB) probed using indicated antibodies. RSPO1 association with LGR4-ECD served as a positive control. (c) Co-IP analysis of LGR4 and RANKL association in HEK293T cells. Western blots probed using indicated antibodies. (d) Co-IP analysis of Δ NT and Δ NT-LRR1 of LGR4-ECD-Flag and RANKL or RSPO1 association in HEK293T cells. (e) Co-IP analysis of NT-LRR17-Flag, NT-LRR14-Flag, and NT-LRR8-Flag of LGR4 association with RANKL or RSPO1 in HEK293T cells. (f–h) SPR binding-affinity measurement of RANKL and three LGR4-ECD deletion mutants. RANKL and NT-LRR17 (LGR4-ECD) binding affinity is 52.2 nM (f). The binding affinity between NT-LRR14 and RANKL is 36.3 nM (kinetic analysis) or 1.527 μ M (affinity analysis) (g). No binding between NT-LRR8 and RANKL was detected (h). (i) Immunofluorescence of LGR4 (green) and RANKL (red) in HEK293T cells. RANKL co-localization with RANK, and RSPO1 co-localization with LGR4, were performed as positive controls. Scale bars, 10 μ m. Representative images of three fields of view per experiment are shown. Images are representative of more than ten experiments (b), three experiments (c,d), and more than three experiments (e,i) with biological replicate. Each co-IP was performed once per experiment and blotted separately each time.

RANKL directly interacts with human LGR4. First, by using a co-immunoprecipitation approach, we found that both the Flag-tagged extracellular domain (ECD) of LGR4 (amino acids (aa) 28–528; LGR4-ECD or N-terminal (NT)-LRR17) (Fig. 1a) and the Flag-tagged full-length LGR4 (LGR4-Flag) physically interact with RANKL (Fig. 1b,c and Supplementary Fig. 1a). Given that the NT domain and leucine-rich repeat domains (LRRs) 1–8 of LGR family proteins are essential for binding to R-spondins 1–4 (RSPOs)^{15,25}, we made four Flag-tagged deletion constructs to examine the LGR4–RANKL interaction (Fig. 1a). Δ NT-Flag (58–528 aa) and Δ NT-LRR1-Flag (80–528 aa) of LGR4 interacted with RANKL but not with RSPO1 (Fig. 1d). The NT-LRR8-Flag of LGR4 (28–249 aa) was associated with RSPO1 but not with RANKL (Fig. 1e). However, the NT-LRR14-Flag of LGR4 (28–396 aa) was associated with RANKL (Fig. 1e). Therefore, different binding motifs are employed in the LGR4–RANKL and the LGR4–RSPO interactions.

Second, by using surface plasmon resonance (SPR) analysis, we found that the NT-LRR17 of LGR4 (LGR4-ECD) bound to RANKL in a dose-dependent manner, with a K_D , a measure of the affinity between the two molecules, of 52.2 nM (Fig. 1f), with OPG protein serving as a positive control (Supplementary Fig. 1b). The K_D between NT-LRR14 and RANKL was 1.527 μ M, whereas no binding was detected between NT-LRR8 and RANKL (Fig. 1g,h and Supplementary Fig. 1c,d). Moreover, OPG inhibited the LGR4-ECD–RANKL interaction (Supplementary Fig. 1e), which suggests that the LGR4-ECD specifically binds to RANKL.

Third, we generated a computational, 3D, complex structural model of RANKL (161–316 aa) and LGR4-ECD (25–528 aa) (Supplementary Fig. 1f,g). The predicted LGR4-ECD interface region was 108–346 aa,

which was consistent with our experimental data (Fig. 1d–h). Because the predicted LGR4–RANKL interaction interface partially overlapped with the interface of LGR4–RSPO, we then examined whether RANKL competed with RSPO1 to interact with LGR4. Our results showed that RSPO1 suppressed the LGR4–RANKL interaction in a dose-dependent manner (Supplementary Fig. 2a).

Fourth, we found that RANKL co-localized with LGR4 on the plasma membrane of human embryonic kidney (HEK) 293T cells expressing LGR4, but did not do so in cells lacking LGR4 (Fig. 1i). Finally, we quantified RANKL binding to LGR4 in HEK293T cells. RANKL binding to cells that overexpressed LGR4 (143.54%) was higher than that to control HEK293T cells (100%) (Supplementary Fig. 2b). Conversely, HEK293T cells with knockdown of endogenous LGR4 had lower RANKL binding (60.37%) than did control cells (100%) (Supplementary Fig. 2c). Furthermore, LGR4-ECD protein inhibited RANKL binding to LGR4-positive HEK293T cells in a dose-dependent manner (Supplementary Fig. 2d). We also examined possible RANK–LGR4 interactions. RANK did not associate with LGR4, either with or without RANKL stimulation (Supplementary Fig. 2e,f). Collectively, our data suggest that RANKL directly binds LGR4.

LGR4 activates $G\alpha_q$ - Ca^{2+} signaling in response to RANKL

LGR4 is predicted to be a GPCR on the basis of its structural homology to rhodopsin-type GPCRs. However, previously reported LGR4 ligands—RSPOs and Norrie disease (NDP, also known as norrin)—fail to induce G-protein signaling^{14,15,26}. Therefore, we investigated whether the binding of RANKL to LGR4 activated heterotrimeric G-protein signaling. RANKL dose-dependently stimulated serum response element (SRE)-luciferase reporter-gene expression in an

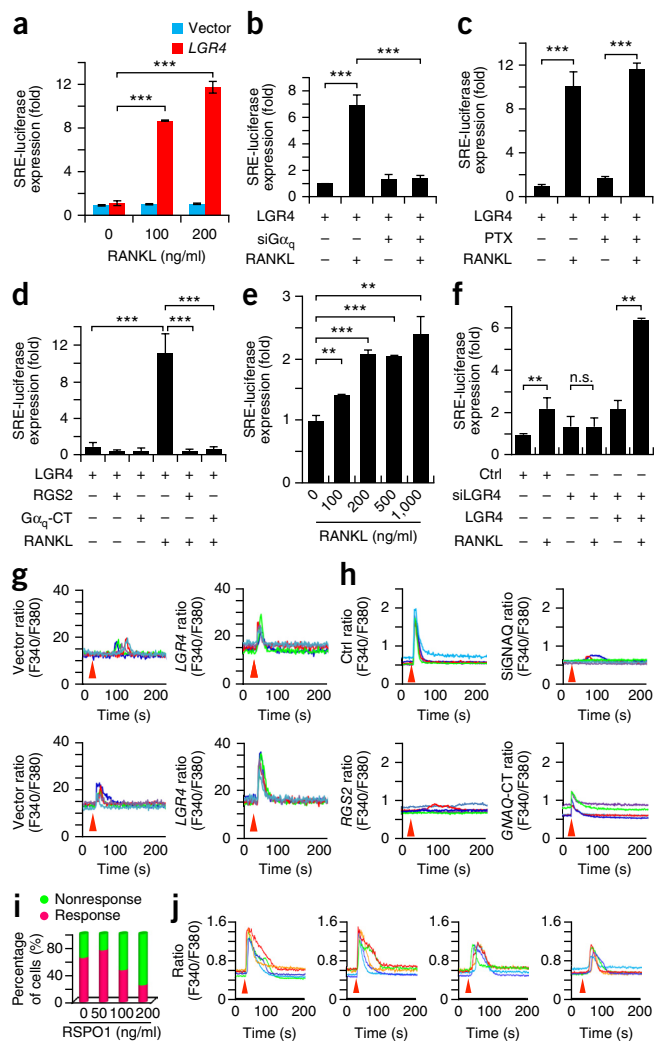
Figure 2 LGR4 activates $G\alpha_q$ -mediated calcium signaling in response to RANKL. **(a)** SRE-luciferase reporter assay in HEK293T cells. **(b–d)** SRE-luciferase expression of HEK293T cells treated with siGNAQ (siRNA targeting *GNAQ*) **(b)**, pertussis toxin PTX (100 ng/ml) **(c)**, or transfected with vectors expressing RGS2 or $G\alpha_q$ -CT **(d)**. **(e)** SRE-luciferase expression in HEK293T cells expressing endogenous LGR4 and siRNA-mediated RANK knockdown, then treated with indicated RANKL concentration. **(f)** SRE-luciferase expression in HEK293T cells with RANK knockdown and indicated treatments. RANKL (1×10^3 ng/ml). n.s., not significant. **(g, h, j)** Calcium imaging of HEK293T cells transfected and treated as indicated. **(g)** Top, 100 ng/ml RANKL; bottom, 200 ng/ml RANKL. **(h)** LGR4 (all groups). **(j)** LGR4 + siRANK + pre-incubation with 0, 50, 100, or 200 ng/ml RSP01 (left to right). Red arrow, time of RANKL stimulation (200 ng/ml unless otherwise specified); colored lines indicate five different representative cells. Each experiment was performed more than three times, and representative results of more than 50 cells per experiment are shown. **(i)** HEK293T cells with (red) or without (green) a RANKL–LGR4-induced calcium response after RSP01 pretreatment. More than 100 cells analyzed in each group. **(a–f)** Error bars are mean \pm s.d. ** $P < 0.01$; *** $P < 0.001$; unpaired two-tailed Student's *t* test. $n = 3$ per group with biological replicates.

LGR4-dependent manner (Fig. 2a), without affecting cAMP-response element (CRE)-, nuclear factor of activated T cell response element (NFAT)- or serum response factor–response element (SRF-RE)-luciferase reporter gene expression, and without altering the production of cAMP (Supplementary Fig. 3a,b). Moreover, siRNA-mediated knockdown of guanine-nucleotide binding protein (G protein), q polypeptide (encoded by *GNAQ*) blocked RANKL-induced SRE-luciferase reporter gene expression, whereas treatment with the G-protein subunit alpha i (encoded by *GNAI1*) inhibitor PTX had little effect on RANKL-induced SRE-driven reporter expression (Fig. 2b,c). Similarly, transfection of either the regulator of G-protein signaling 2 (RGS2) or the C-terminal domain of $G\alpha_q$ ($G\alpha_q$ -CT), both of which selectively block $G\alpha_q$ activation²⁷, inhibited RANKL-induced reporter-gene expression (Fig. 2d). RANKL also stimulated SRE-luciferase reporter-gene expression in a dose-dependent manner through endogenous LGR4 in HEK293T cells (Fig. 2e). We also found that siRNA-mediated *LGR4* knockdown blocked the induction of SRE-luciferase by RANKL, whereas co-transfection with an *LGR4*-expression plasmid restored RANKL-induced SRE-promoter activation (Fig. 2f).

Because $G\alpha_q$ activation leads to intracellular calcium release²⁸, we subsequently used calcium imaging to examine whether RANKL induces intracellular calcium release through LGR4. RANKL markedly stimulated calcium release in LGR4-overexpressing cells in a concentration-dependent manner, in contrast to the mild calcium release induced in control cells (Fig. 2g). Similar results were obtained with a fluorescence-imaging plate reader (FLIPR) calcium assay (Supplementary Fig. 3c). Consistently with our luciferase-assay results, all three $G\alpha_q$ blockers—RGS2, $G\alpha_q$ -CT, and siRNA of *GNAQ*—almost completely blocked RANKL-induced calcium release (Fig. 2h). Furthermore, RSP01 dose-dependently suppressed RANKL–LGR4-triggered calcium release (Fig. 2i,j). Therefore, our results indicate that RANKL triggers LGR4-mediated signaling via $G\alpha_q$.

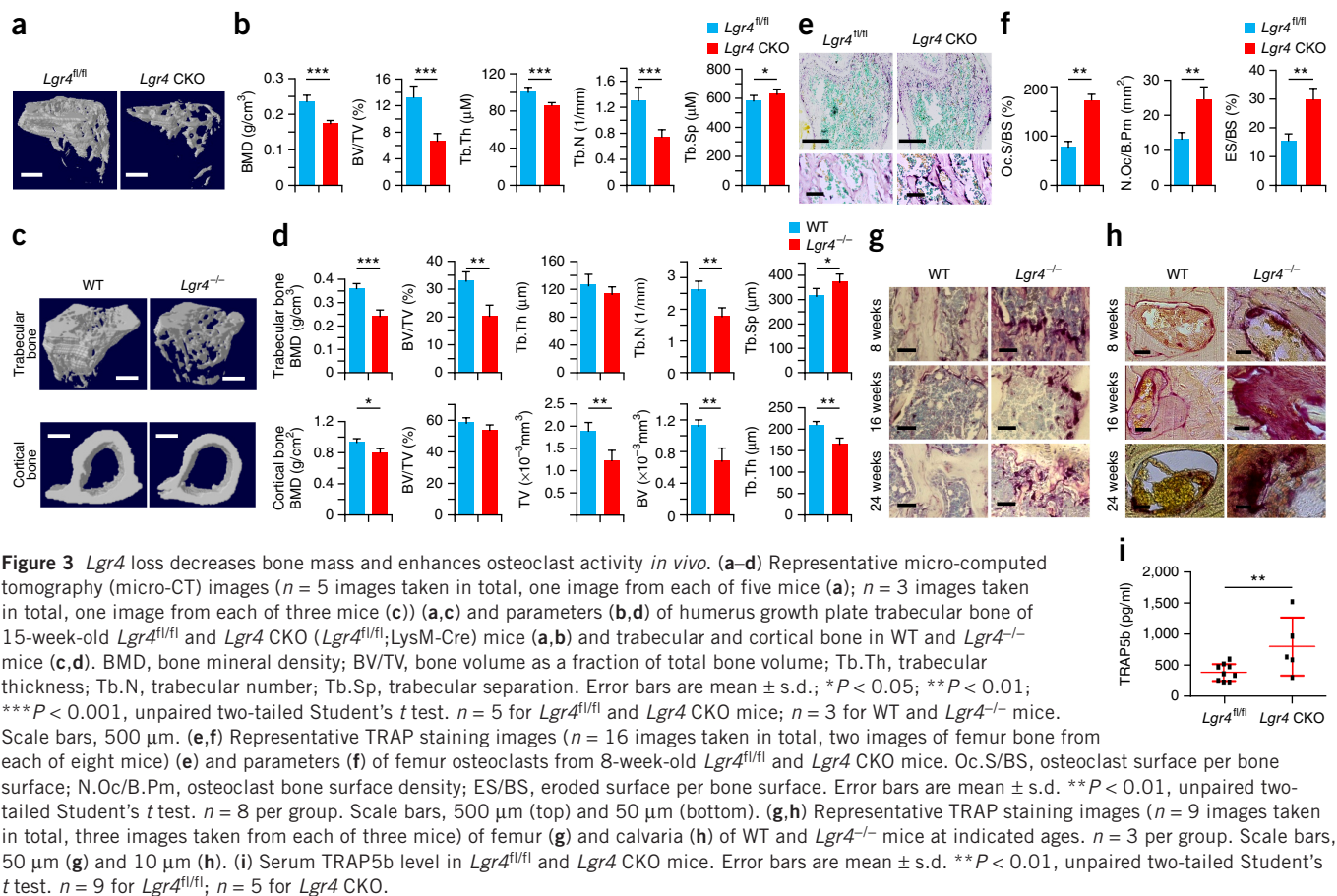
Lgr4 loss decreases bone mass and enhances osteoclast activity

RANKL is recognized as the key factor in osteoclastogenesis¹. A nonsense mutation in *LGR4* is correlated with low BMD in humans¹⁶. We therefore tested whether the RANKL–LGR4 interaction affects osteoclast differentiation and function in mice. Several LGR family members participate in bone remodeling^{13,16–18}; only the expression of *Lgr4*, however, was dramatically induced during RANKL-driven



osteoclast differentiation (Supplementary Fig. 4a). We confirmed LGR4 expression in osteoclasts by LacZ and TRAP co-staining bone sections from *Lgr4*^{+/-} mice, which have the β -gal transcript knocked into the *Lgr4* locus¹³ (Supplementary Fig. 4b). Furthermore, *Lgr4* is a transcriptional target of RANKL–NFATc1 signaling during osteoclastogenesis (Supplementary Fig. 4c–g), which suggests that LGR4 could be a novel regulator during osteoclastogenesis.

To understand the functions of *Lgr4* *in vivo*, we examined the bone phenotypes of mice deficient in *Lgr4* (*Lgr4*^{-/-} and *Lgr4* CKO). Both mouse models exhibited low BMD (Fig. 3a–d and Supplementary Fig. 5a,b), which is consistent with the human phenotype¹⁶. Moreover, bone loss was exacerbated as the mice aged from 8 to 15 weeks old (data not shown). In a manner consistent with our observations of an increase in bone loss, we found greater numbers of TRAP-positive osteoclasts and larger osteoclast size in the femoral bones and calvaria of *Lgr4*^{-/-} and *Lgr4* CKO mice, as compared to those in wild-type mice, at all ages analyzed (Fig. 3e–h), which suggests that osteoclasts in *Lgr4*-deficient mice are hyperactivated. Bone-morphometric analysis revealed that osteoclast surface, osteoclast number, osteoclast size, and eroded surface were all markedly higher in *Lgr4*^{-/-} and *Lgr4* CKO mice than in control mice (Fig. 3f and Supplementary Table 1). Moreover, the serum-bone resorption (osteoclast) marker acid phosphatase 5, tartrate resistant (TRAP5b) was significantly higher in *Lgr4* CKO mice than in control wild-type mice (Fig. 3i; $P < 0.01$), whereas no



significant difference was observed in the serum bone-formation (osteoblast) markers procollagen I NT propeptide (PINP) and osteocalcin (data not shown). This suggests that osteoclast hyperactivation was the main reason for low bone mass in *Lgr4*-deficient mice.

Lgr4 loss enhances the formation and blocks apoptosis of osteoclasts

We next examined LGR4 in osteoclast differentiation *in vitro*. RANKL treatment resulted in notably greater osteoclast number and size in bone marrow monocytes (BMMs) from *Lgr4* CKO mice (Fig. 4a), in *Lgr4*^{-/-} BMMs (Supplementary Fig. 6a), and in *Lgr4*-knockdown pre-osteoclast RAW264.7 cells (Supplementary Fig. 6b) than in cells from control mice. Conversely, ectopic *Lgr4* expression in RAW264.7 cells resulted in a lower number of and smaller-sized osteoclasts than those in vector-treated control cells (Supplementary Fig. 6c). The loss of *Lgr4* also rendered BMMs more responsive than control BMMs to doses of RANKL lower than the standard dose (Fig. 4a). Moreover, *Lgr4* loss accelerated BMM differentiation, especially in later stages (Fig. 4b), probably owing to increased *Lgr4* expression levels during BMM differentiation (Supplementary Fig. 4a,b). *Lgr4* loss in osteoclasts deregulated bone resorption, with *Lgr4*^{-/-} BMMs generating more pits with greater pit depth, perimeter, and area than those in BMMs from wild-type mice (Fig. 4c–e; $P < 0.01$). Osteoclast marker gene profiling in wild-type (WT) and *Lgr4*^{-/-} osteoclasts also indicated that osteoclast formation (as determined by the expression of *Nfatc1*; of acid phosphatase 5, tartrate resistant (*Acp5*); and of Rous sarcoma oncogene (*Src*) and resorption (as determined by the expression of calcitonin receptor (*Calcr*) and cathepsin K (*Ctsk*)) were enhanced in *Lgr4*^{-/-} BMMs (Supplementary Fig. 6d).

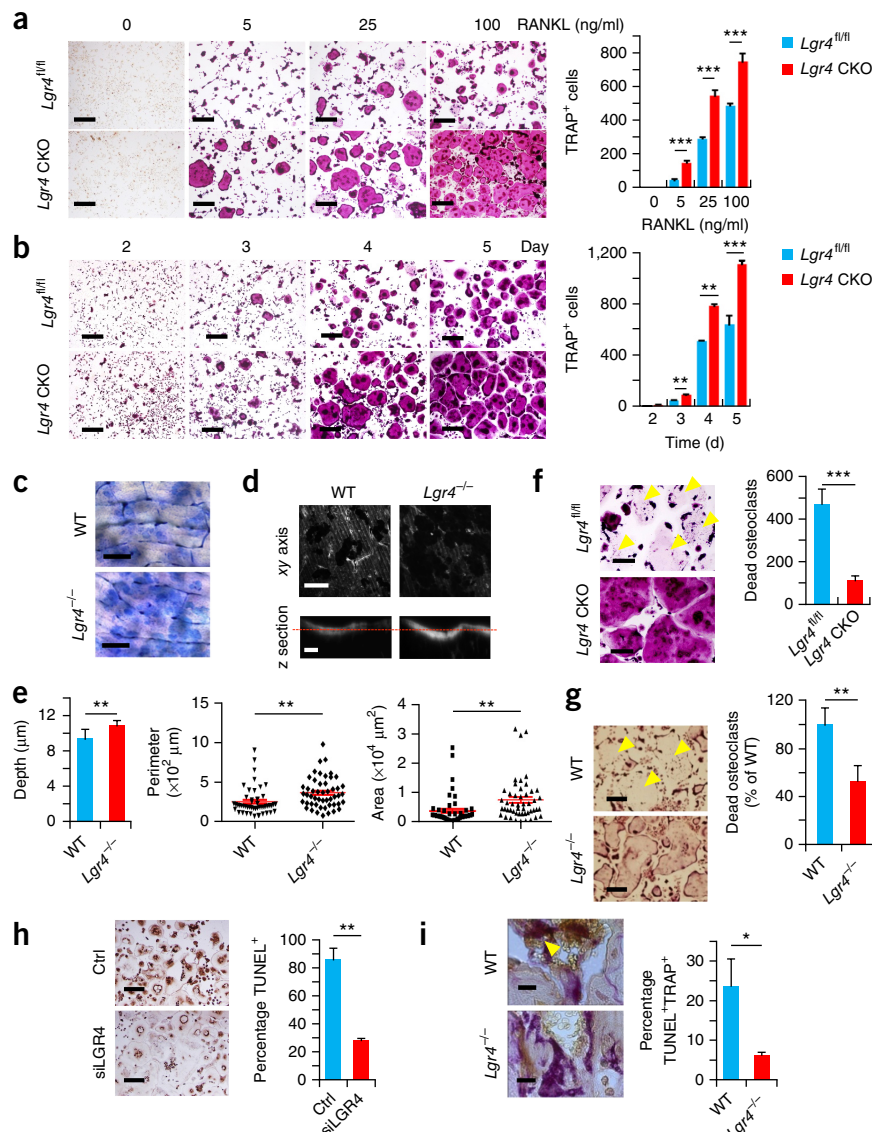
Because RANKL is an important survival factor for osteoclasts²⁹, we determined whether LGR4 also influences osteoclast survival *in vitro*. The number of dead cells in 8-day cultures of BMMs from both *Lgr4*^{-/-} and *Lgr4* CKO mice (i.e., mature osteoclasts) was markedly lower than in those from control osteoclasts (Fig. 4f,g). *Lgr4* knockdown in RAW264.7 cells resulted in substantially fewer dead osteoclasts than did treatment with a control siRNA (Fig. 4h). Similar results were obtained *in vivo* via TUNEL staining of TRAP-positive osteoclasts (Fig. 4i), which suggests that LGR4 regulates osteoclast survival. Therefore, LGR4 inhibits RANKL-induced osteoclast differentiation, survival, and function *in vivo* and *in vitro*.

LGR4 affects the canonical RANK-signaling pathway

To investigate how LGR4 functions in osteoclastogenesis, we first examined whether RSPOs or norrin affect osteoclastogenesis. None of the reported LGR4 ligands had any effect on the osteoclast differentiation of BMMs or RAW264.7 cells (Fig. 5a,b and Supplementary Fig. 7a,b), which is consistent with a previous report³⁰. Moreover, neither RSPO nor norrin treatment affected osteoclastogenesis of *Lgr4*-deficient BMMs (Fig. 5a,b). Furthermore, there was no significant difference in BMM differentiation between R-spondin 4 (*Rspo4*)^{+/+}, *Rspo4*^{+/-}, and *Rspo4*^{-/-} mice (Fig. 5c). Taken together, our data suggested that *Lgr4*-deficiency-induced osteoclastogenesis is independent of RSPOs and norrin.

Next, we examined whether LGR4 affects the canonical RANKL–RANK signaling pathway. The LGR4-ECD dose-dependently inhibited RANKL binding to RANK (Fig. 5d), which suggests that LGR4 competes with RANK to interact with RANKL. Consequently,

Figure 4 *Lgr4* loss enhances osteoclast formation and inhibits mature osteoclast apoptosis. (a,b) Representative TRAP staining images (left) ($n = 9$ images taken in total, one image from one well each, with triplicate repeat wells of three biological replicates) of BMM cells isolated from *Lgr4^{fl/fl}* and *Lgr4* CKO mice cultured with colony-stimulating factor 1 (M-CSF, also called CSF1) (10 ng/ml) and either varying RANKL (a) or indicated times with 100 ng/ml RANKL (b). The osteoclast numbers were counted (right). Scale bars, 500 μ m. (c–e) Representative toluidine blue staining images ($n = 4$ images taken in total; two images from each of two biological replicates) of resorption pits generated by mature osteoclasts from indicated mice seeded on bone slices (c). Representative reflection images ($n = 10$ images taken in total, five images from each of two biological replicates) (d) and pit depth, perimeter and area. Error bars are mean \pm s.e.m. (e) of pits scanned by confocal microscopy (xy section and z section). Scale bars, 200 μ m (c and d top) and 10 μ m (d bottom). (f,g) TRAP staining of BMMs from indicated mice cultured with RANKL (100 ng/ml) and M-CSF (10 ng/ml) for 8 d. Representative images ($n = 3$ images taken in total with technical triplicate repeat) (left) and dead osteoclast (yellow arrowheads) quantification (right) from *Lgr4^{fl/fl}* and *Lgr4* CKO mice (f) and WT and *Lgr4^{-/-}* mice (g). Scale bars, 100 μ m (f) and 200 μ m (g). (h) Representative TUNEL-stained images ($n = 9$ images taken in total, three images from one well, each with triplicate repeated wells of three biological replicates) (left) and the proportion of TUNEL-positive, multinucleated osteoclasts (right) of BMMs transfected with indicated siRNAs. Scale bars, 200 μ m. (i) Femurs from WT and *Lgr4^{-/-}* mice were stained for TRAP and TUNEL. Scale bars, 10 μ m. Representative images ($n = 12$ images taken in total, four images from each of three mice) (left) and TUNEL- and TRAP-double-positive cell quantitation (right). In each panel except perimeter and area in (e), error bars are mean \pm s.d. * $P < 0.05$, ** $P < 0.01$, *** $P < 0.001$, unpaired two-tailed Student's *t* test, $n = 3$ per group except c–e, where $n = 50$ per group.



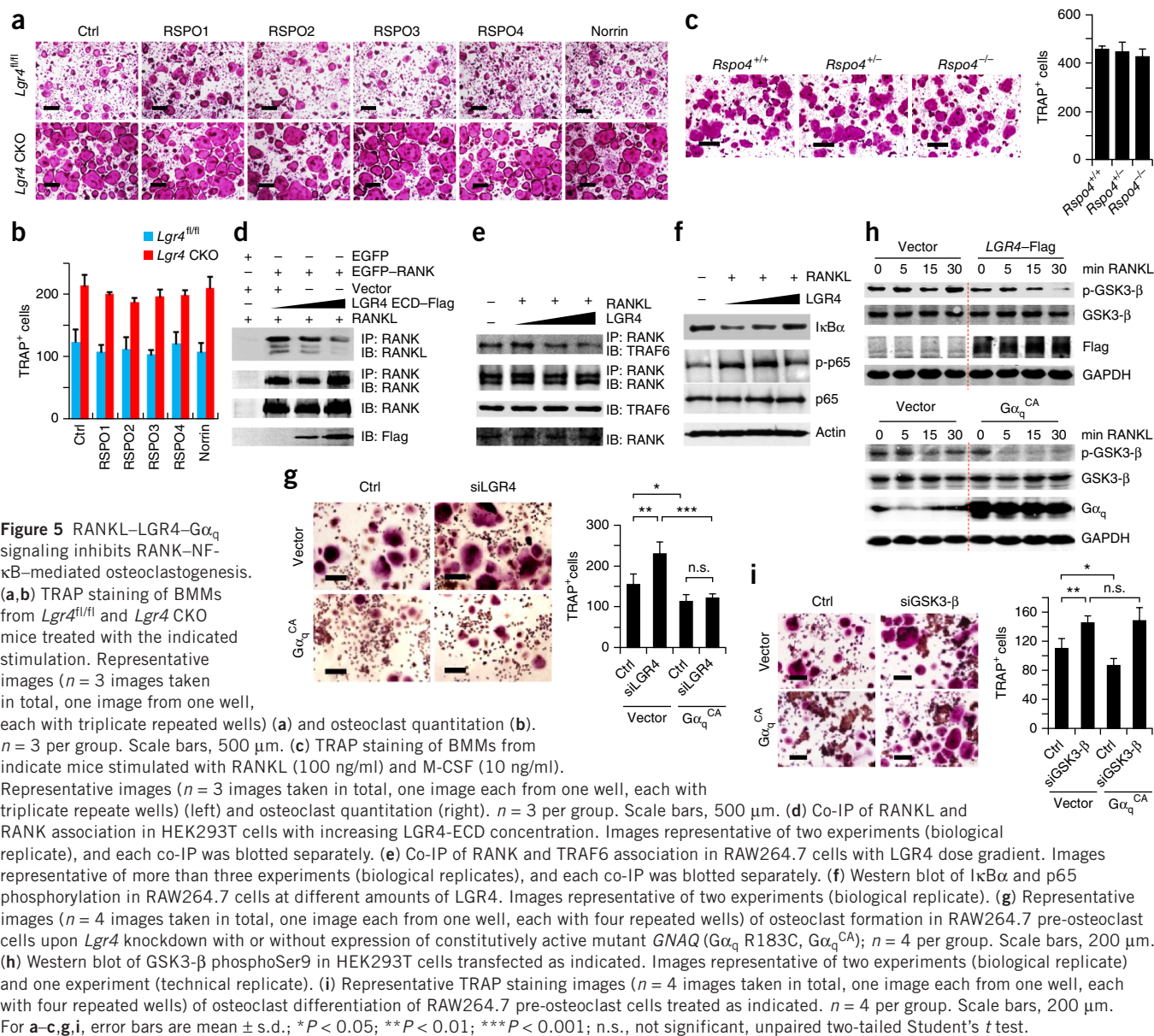
LGR4 attenuated RANKL-induced association of RANK with its key downstream signaling molecule TRAF6 in a dose-dependent manner (Fig. 5e). Furthermore, LGR4 abrogated RANKL-induced NF- κ B signaling by decreasing the phosphorylation of NF- κ B or p65 and by inhibiting the degradation of NFKB inhibitor- α (I κ B α , also called NFKBIA) (Fig. 5f and Supplementary Fig. 7c).

RANKL–LGR4–G α_q –GSK3- β –NFATC1 pathway blocks osteoclastogenesis

We next determined whether LGR4–G α_q signaling regulates osteoclastogenesis. Knockdown or overexpression of *GNAQ*, similarly to changes in *Lgr4* expression, showed that G α_q negatively regulated osteoclast differentiation (data not shown). Moreover, overexpression of constitutively active G α_q (G α_q^{CA}) prevented *Lgr4*-knockdown-induced osteoclast differentiation (Fig. 5g). G α_q signaling also negatively regulated the expression of NFATC1, the key transcription factor in osteoclastogenesis, and its downstream target

genes (Supplementary Fig. 7d and data not shown). Moreover, G α_q inhibited RANKL-induced NFATC1 nuclear translocation (Supplementary Fig. 7d), most probably via the inhibition of glycogen synthase kinase 3- β (GSK3- β) serine 9 (Ser9) phosphorylation³¹ (Fig. 5h). The overexpression of either *RGS2* or *GNAQ-CT* restored GSK3- β Ser9 phosphorylation (Supplementary Fig. 7e). In addition, RANKL-induced GSK3- β Ser9 phosphorylation occurred in *Rank* knockout cells (Supplementary Fig. 7f), which suggests that RANKL-induced GSK3- β Ser9 phosphorylation is independent of RANK expression.

To confirm the relevance of this pathway in osteoclastogenesis, we investigated whether knockdown of GSK3- β can normalize osteoclast differentiation suppressed by *GNAQ* overexpression. We observed that *Gsk3- β* knockdown by siRNA rescued the inhibition of osteoclast differentiation in G α_q^{CA} -overexpressing cells (Fig. 5i). These data show that LGR4–G α_q signaling affects RANKL-induced osteoclastogenesis.



Soluble LGR4-ECD protein ameliorates bone loss

RANKL blockade has been effective in treating multiple diseases that result in bone loss, including osteoporosis¹¹. Therefore, we examined whether soluble LGR4-ECD protein, which contains the RANKL interaction domain, could ameliorate osteoporosis. We validated that LGR4-ECD suppressed RSPO1-induced top- and fop-FLASH luciferase-reporter expression in a concentration-dependent manner (data not shown). We then used four models of osteoclast differentiation *in vitro* to determine the effect of LGR4-ECD protein on osteoclast development. In all four models, LGR4-ECD inhibited osteoclast development in a dose-dependent manner (Fig. 6a,b and Supplementary Fig. 7g,h). LGR4-ECD had little effect on the survival of osteoblasts and osteoclasts, and it did not alter the RANKL/OPG ratio in osteoblast cells (data not shown).

To evaluate the potential effect of LGR4-ECD on osteoporosis *in vivo*, we employed three osteoporosis mouse models: ovariectomy, RANKL injection³² and *Tnfrsf11b*-deficient mice³³. In ovariectomized mice, administration of the LGR4-ECD notably increased bone mass

and decreased osteoclast activity, relative to control-treated mice (Fig. 6c-f). Similarly, LGR4-ECD treatment decreased osteoclast activity and increased bone mass in both RANKL injection and *Tnfrsf11b*-deficient mouse models (Fig. 6g-i and Supplementary Fig. 8a-g). LGR4-ECD alone had little effect on osteoclast activity or on bone mass in healthy mice (Fig. 6g-i and Supplementary Fig. 8a-c), and their body weight was unchanged (data not shown). Thus, LGR4-ECD acts as a molecular decoy receptor for RANKL both *in vitro* and *in vivo*, and inhibits RANKL-induced osteoclast activation and bone loss.

DISCUSSION

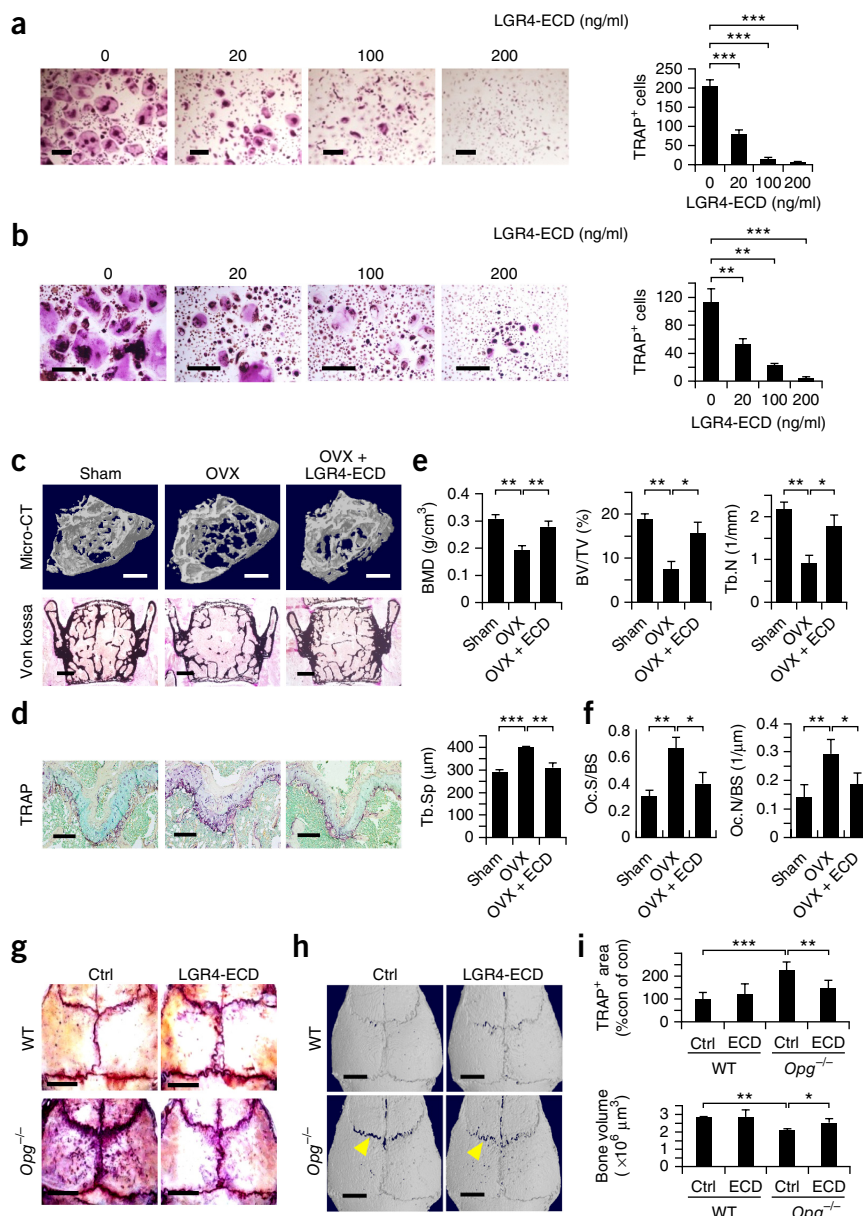
We here show that LGR4 is a novel RANKL receptor that competes with RANK for RANKL binding in osteoclasts. LGR4 inhibits RANKL-induced osteoclast differentiation by blocking RANK-TRAF6 signaling, as well as through $G\alpha_q$ -mediated inhibition of NFATC1. Furthermore, LGR4 is a downstream target of RANKL-RANK signaling, which suggests that LGR4 functions in a negative feedback

Figure 6 Soluble LGR4-ECD protein ameliorates bone loss in the RANKL-injection and *Tnfrsf11b*-knockout osteoporosis mouse models.

(a) Representative TRAP staining images (left) ($n = 3$ images taken in total, one image each from one well, each with triplicated repeated wells) of mouse BMMs cultured with RANKL, M-CSF, and soluble LGR4-ECD protein.

The osteoclast numbers were counted (right). Error bars are mean \pm s.d.; *** $P < 0.001$, unpaired two-tailed Student's *t* test. $n = 3$ per group. Scale bars, 500 μ m. (b) Representative TRAP staining images (left) ($n = 24$ images taken in total, four images each from one well, each with triplicated repeated wells of two biological replicates) of human peripheral blood mononuclear cells (PBMC) cultured with RANKL, M-CSF, and soluble LGR4-ECD protein. The osteoclast numbers were counted (right). Error bars are mean \pm s.d.; ** $P < 0.01$, *** $P < 0.001$, unpaired two-tailed Student's *t* test. $n = 3$ per group. Scale bars, 500 μ m.

(c–f) Representative micro-CT images ($n = 8$ images taken in total, one image from eight different mice each) (c) and TRAP staining images ($n = 16$ images taken in total, two images from eight different mice each) (d) of the femur and representative L3 lumbar images ($n = 16$ images taken in total, two images each from eight different mice) (c, bottom) and histomorphometric analysis (e) of control (sham) and ovariectomized (OVX) mice treated with or without LGR4-ECD. Error bars are mean \pm s.d. * $P < 0.05$, ** $P < 0.01$, *** $P < 0.001$, unpaired two-tailed Student's *t* test. $n = 8$ per group. Scale bars, 500 μ m (c) and 200 μ m (d). (g–i) Representative TRAP staining images ($n = 6$ images taken in total, one image each from six different mice) (g), representative micro-CT images ($n = 6$ images taken in total, one image each from six different mice) (h) and parameter analysis (i) of whole calvaria from wild-type (WT) and *Tnfrsf11b*^{-/-} mice treated with either control (Ctrl) or LGR4-ECD (ECD) protein (1 mg/kg/day) daily for 2 weeks. Arrowheads indicate bone erosion. Error bars are mean \pm s.d. * $P < 0.05$, ** $P < 0.01$, *** $P < 0.001$, unpaired two-tailed Student's *t* test. $n = 6$ per group. Scale bars, 2 mm.



loop to limit RANKL osteoclastogenesis and to reduce the numbers of osteoclasts *in vivo*. The injection of soluble LGR4-ECD inhibited osteoclast differentiation *in vitro* and osteoporosis in three mouse models, which suggests that this may be a viable strategy for the treatment of osteoporosis and other bone-resorption diseases in humans.

RANKL regulates osteoclast survival by reducing the expression of the death receptor *Fas* in mature osteoclasts^{29,34–36}. However, mature osteoclasts ultimately undergo apoptosis in a RANKL-containing environment³⁷, which suggests the existence of a RANKL-induced signaling pathway that limits the survival of mature osteoclasts. Our data implicate LGR4 as a crucial component of a negative-feedback mechanism to limit osteoclast function *in vivo*. LGR4 expression is induced by RANKL–NFATC1 signaling during osteoclast differentiation. In mature osteoclasts, the expression level of *Lgr4* is especially elevated, which indicates that LGR4 inhibition of RANKL–RANK binding reaches a peak and thus results in decreased RANKL–RANK signaling, increased *Fas* expression, and apoptosis induction

(Supplementary Fig. 8h). This mechanism could explain why mature osteoclasts still undergo apoptosis with RANKL present, and why the loss of *Lgr4* prolongs osteoclast survival.

We previously found that *Lgr4* affects bone development by regulating osteoblast differentiation¹³, potentially affecting bone mass via osteoblast regulation. However, using monocyte-specific *Lgr4*-knockout mice, our data here show that *Lgr4* CKO mice had similar phenotypes to global *Lgr4* knockout mice, including strikingly decreased bone mass, and sharply increased osteoclast differentiation and bone resorption, as compared to control mice, *in vivo* and *in vitro*. Although our results here do not preclude the contribution of osteoblast dysregulation to the *Lgr4*^{-/-} decreased bone mass phenotype, they do suggest that osteoclast *Lgr4*-deficiency predominates in driving the low bone mass seen in mice and humans with an *LGR4* mutation¹⁶.

OPG-Fc protein and denosumab are two well-known RANKL-binding agents developed to treat osteoclast-related diseases, including osteoporosis¹¹. The truncated OPG protein (OPG-Fc),

which is 200-fold more efficient than full-length OPG, was discontinued owing to the possibility of a neutralizing immune response to endogenous OPG in individuals¹¹. Denosumab, a human monoclonal antibody against RANKL, has many side effects, including calcium homeostasis imbalance and hypocalcemia. Here we show that LGR4-ECD protein had a lower binding affinity than OPG with RANKL, and that LGR4-ECD protein had little physiological effect on osteoclast differentiation in normal mice, which suggests that the minimal effect of LGR4-ECD protein in normal mice could be due to endogenous OPG competition. We speculate that in pathological conditions, LGR4-ECD could antagonize excessive RANKL with few side effects because it lacks any effects on normal physiological function. Furthermore, *Lgr4* expression increased during osteoclast differentiation and peaked in mature osteoclasts; targeting LGR4 thus may affect mature osteoclasts but have less effect in BMMs and pre-osteoclasts, and so reduce side effects involved in the treatment of osteoclast-related diseases.

In addition to regulating osteoclast differentiation, RANKL has crucial roles in many other processes, including in mammary gland development during pregnancy and in lactation^{3,5}. It is also implicated in progesterone-induced breast carcinogenesis⁵, and in breast cancer bone metastasis⁴. We have recently identified LGR4 as a key regulator in mammary stem cell maintenance²⁰. We speculate that the RANKL–LGR4 interaction identified here may link mammary stem cells to breast cancer initiation and metastasis, as well as to alveolar development during pregnancy. Further research is urgently needed to resolve this question and to investigate LGR4 mediation of RANKL signaling in other systems, including immune response, or in diabetes.

METHODS

Methods and any associated references are available in the [online version of the paper](#).

Note: Any Supplementary Information and Source Data files are available in the online version of the paper.

ACKNOWLEDGMENTS

This work is supported by grants from the National Basic Research Program of China (2012CB910402 to J.L.; 2012CB910400 to M.L.), the National Natural Science Foundation of China (81472048, 81272911 to J.L.; 81330049 to M.L.; 81522011 to J.W.), the Science and Technology Commission of Shanghai Municipality (15140903600 to J.L.), and the Innovation Program of Shanghai Municipal Education Commission (14ZZ051 to J.L.). The advanced ERC grant and an Era of Hope/DoD innovator award were given to JMP. We thank G. Ning (Ruijin Hospital, Shanghai JiaoTong University School of Medicine) for the *Lgr4*^{flxed} mice, J. Penninger (Institute of Molecular Biotechnology of the Austrian Academy of Sciences) for the *Rank*^{flxed} mice, and Y. Zhang (Shanghai East Hospital, Tongji University School of Medicine) for the *LysM-Cre* mice.

AUTHOR CONTRIBUTIONS

J.L. and Z. Yang generated the initial idea, proposed the hypothesis, and designed the study. Z. Yang conducted the key experiments. J.L. and M.L. supervised the study and performed the data analysis, interpreted results and wrote the manuscript. Y.M., Z. Yue, H.L., G.Q., J.H., C.L., and C.Z., performed the experiments. W.D. performed the docking and molecular modeling. L.X. and J.X. prepared and analyzed human samples. H.C., J.W., D.L., S.S., J.M.P., and G.N. provided the animals and analyzed the animal data. S.S. and J.M.P. analyzed data and wrote the manuscript.

COMPETING FINANCIAL INTERESTS

The authors declare no competing financial interests.

Reprints and permissions information is available online at <http://www.nature.com/reprints/index.html>.

1. Kong, Y.Y. *et al.* OPG is a key regulator of osteoclastogenesis, lymphocyte development and lymph-node organogenesis. *Nature* **397**, 315–323 (1999).

2. Hanada, R., Hanada, T., Sigl, V., Schramek, D. & Penninger, J.M. RANKL/RANKL beyond bones. *J. Mol. Med.* **89**, 647–656 (2011).
3. Fata, J.E. *et al.* The osteoclast differentiation factor osteoprotegerin-ligand is essential for mammary gland development. *Cell* **103**, 41–50 (2000).
4. Jones, D.H. *et al.* Regulation of cancer cell migration and bone metastasis by RANKL. *Nature* **440**, 692–696 (2006).
5. Gonzalez-Suarez, E. *et al.* RANK ligand mediates progesterin-induced mammary epithelial proliferation and carcinogenesis. *Nature* **468**, 103–107 (2010).
6. Tan, W. *et al.* Tumour-infiltrating regulatory T cells stimulate mammary cancer metastasis through RANKL-RANK signalling. *Nature* **470**, 548–553 (2011).
7. Schramek, D. *et al.* Osteoclast differentiation factor RANKL controls development of progesterin-driven mammary cancer. *Nature* **468**, 98–102 (2010).
8. Kiechl, S. *et al.* Blockade of receptor activator of nuclear factor- κ B (RANKL) signaling improves hepatic insulin resistance and prevents development of diabetes mellitus. *Nat. Med.* **19**, 358–363 (2013).
9. Hanada, R. *et al.* Central control of fever and female body temperature by RANKL/RANK. *Nature* **462**, 505–509 (2009).
10. Simonet, W.S. *et al.* Osteoprotegerin: a novel secreted protein involved in the regulation of bone density. *Cell* **89**, 309–319 (1997).
11. Lacey, D.L. *et al.* Bench to bedside: elucidation of the OPG-RANK-RANKL pathway and the development of denosumab. *Nat. Rev. Drug Discov.* **11**, 401–419 (2012).
12. Weng, J. *et al.* Deletion of G protein-coupled receptor 48 leads to ocular anterior segment dysgenesis (ASD) through down-regulation of Pitx2. *Proc. Natl. Acad. Sci. USA* **105**, 6081–6086 (2008).
13. Luo, J. *et al.* Regulation of bone formation and remodeling by G-protein-coupled receptor 48. *Development* **136**, 2747–2756 (2009).
14. Carmon, K.S., Gong, X., Lin, Q., Thomas, A. & Liu, Q. R-spondins function as ligands of the orphan receptors LGR4 and LGR5 to regulate Wnt/beta-catenin signaling. *Proc. Natl. Acad. Sci. USA* **108**, 11452–11457 (2011).
15. de Lau, W. *et al.* Lgr5 homologues associate with Wnt receptors and mediate R-spondin signalling. *Nature* **476**, 293–297 (2011).
16. Strykarsdotir, U. *et al.* Nonsense mutation in the LGR4 gene is associated with several human diseases and other traits. *Nature* **497**, 517–520 (2013).
17. Abe, E. *et al.* TSH is a negative regulator of skeletal remodeling. *Cell* **115**, 151–162 (2003).
18. Sun, L. *et al.* FSH directly regulates bone mass. *Cell* **125**, 247–260 (2006).
19. Du, B. *et al.* Lgr4/Gpr48 negatively regulates TLR2/4-associated pattern recognition and innate immunity by targeting CD14 expression. *J. Biol. Chem.* **288**, 15131–15141 (2013).
20. Wang, Y. *et al.* Lgr4 regulates mammary gland development and stem cell activity through the pluripotency transcription factor Sox2. *Stem Cells* **31**, 1921–1931 (2013).
21. Wang, J. *et al.* Ablation of LGR4 promotes energy expenditure by driving white-to-brown fat switch. *Nat. Cell Biol.* **15**, 1455–1463 (2013).
22. Gao, Y. *et al.* Up-regulation of GPR48 induced by down-regulation of p27Kip1 enhances carcinoma cell invasiveness and metastasis. *Cancer Res.* **66**, 11623–11631 (2006).
23. Wu, J. *et al.* GPR48, a poor prognostic factor, promotes tumor metastasis and activates β -catenin/TCF signaling in colorectal cancer. *Carcinogenesis* **34**, 2861–2869 (2013).
24. Joshi, P.A. *et al.* RANK signaling amplifies WNT-responsive mammary progenitors through R-SPONDIN1. *Stem Cell Reports* **5**, 31–44 (2015).
25. Wang, D. *et al.* Structural basis for R-spondin recognition by LGR4/5/6 receptors. *Genes Dev.* **27**, 1339–1344 (2013).
26. Deng, C. *et al.* Multi-functional norrin is a ligand for the LGR4 receptor. *J. Cell Sci.* **126**, 2060–2068 (2013).
27. Tang, X. *et al.* GPR116, an adhesion G-protein-coupled receptor, promotes breast cancer metastasis via the G α q-p63RhoGEF-Rho GTPase pathway. *Cancer Res.* **73**, 6206–6218 (2013).
28. Clapham, D.E. Calcium signaling. *Cell* **131**, 1047–1058 (2007).
29. Wu, X. *et al.* RANKL regulates Fas expression and Fas-mediated apoptosis in osteoclasts. *J. Bone Miner. Res.* **20**, 107–116 (2005).
30. Krönke, G. *et al.* R-spondin 1 protects against inflammatory bone damage during murine arthritis by modulating the Wnt pathway. *Arthritis Rheum.* **62**, 2303–2312 (2010).
31. Moon, J.B. *et al.* Akt induces osteoclast differentiation through regulating the GSK3 β /NFATc1 signaling cascade. *J. Immunol.* **188**, 163–169 (2012).
32. Takeshita, S. *et al.* Osteoclast-secreted CTHRC1 in the coupling of bone resorption to formation. *J. Clin. Invest.* **123**, 3914–3924 (2013).
33. Mizuno, A. *et al.* Severe osteoporosis in mice lacking osteoclastogenesis inhibitory factor/osteoprotegerin. *Biochem. Biophys. Res. Commun.* **247**, 610–615 (1998).
34. Lacey, D.L. *et al.* Osteoprotegerin ligand modulates murine osteoclast survival *in vitro* and *in vivo*. *Am. J. Pathol.* **157**, 435–448 (2000).
35. Jimi, E. *et al.* Osteoclast differentiation factor acts as a multifunctional regulator in murine osteoclast differentiation and function. *J. Immunol.* **163**, 434–442 (1999).
36. Boyce, B.F. Advances in the regulation of osteoclasts and osteoclast functions. *J. Dent. Res.* **92**, 860–867 (2013).
37. Manolagas, S.C. & Parfitt, A.M. What old means to bone. *Trends Endocrinol. Metab.* **21**, 369–374 (2010).

ONLINE METHODS

Immunoprecipitation analysis. For immunoprecipitation analysis, RAW264.7 cells were transfected with vector or *LGR4* plasmids. After 48 h, cell lysates were prepared with RIPA buffer (1% Nonidet P-40 in 150 mM NaCl, 50 mM Tris-HCl, 0.25% sodium deoxycholate, 2 mM PMSF, pH 7.4) with complete protease-inhibitor cocktail (Roche Applied Science, 04693124001). The supernatant was incubated with RANK (Santa Cruz, sc-9072, 1:50) or TRAF6 (Abcam, ab33915, 1:50) antibodies at 4 °C overnight, which was followed by protein A/G bead incubation for another 3 h at 4 °C. Immune complexes were washed three times with phosphate-buffered saline (PBS) and subjected to western blot analysis using specific antibodies for TRAF6 (Abcam, ab33915, 1:1000) and RANK (Santa Cruz, sc-9072, 1:500). To detect the association of RANKL with LGR4-ECD, RANKL with NT-LRR14 and RANKL with NT-LRR8, HEK293T cells were transfected with indicated plasmids, and cell lysates were prepared with radioimmunoprecipitation assay (RIPA) buffer. The supernatant was incubated with 500 ng RANKL or 200 ng RSPO1-His at 4 °C overnight, and this was followed by incubation with Flag-M2 beads (Sigma-Aldrich, A2220, 5 µl per sample) for another 3 h at 4 °C. Immune complexes were then subjected to western blot using specific antibodies for Flag (Sigma-Aldrich, F7425, 1:2,000), His (Abmart, M30111, 1:5000), or RANKL (IMGENEX, IMG-185A, 1:2,000). To perform the RSPO1 competition experiment, HEK293T cells were transfected with LGR4-ECD plasmids, and cell lysates were prepared with RIPA buffer. The supernatant was incubated with RSPO1-His in 200 ng/ml, 500 ng/ml and 1,000 ng/ml at 4 °C for 12 h, respectively. Then 500 ng RANKL was added, and the complex was followed by incubation with Flag-M2 beads (Sigma-Aldrich, A2220, 5 µl per sample) for another 3 h at 4 °C. Immune complexes were then subjected to western blot using specific antibodies for Flag (Sigma-Aldrich, F7425, 1:2,000), His (Abmart, M30111, 1:5000), or RANKL (IMGENEX, IMG-185A, 1:2,000).

Protein expression and purification. cDNA of human LGR4-ECD (amino acids 25–528) and ΔNT-LRR1 (80–528 aa) were subcloned into the pET28a⁺ vector at the BamHI and EcoRI restriction sites. The pET28a⁺-ECD and pET28a⁺-ΔNT&LRR1 proteins were expressed in *Escherichia coli* (Rosetta DE3), His-ECD and His-ΔNT&LRR1 were purified from *E. coli* lysates under native conditions and purified with the nickel-nitrilotriacetic acid (Ni-NTA) system. Briefly, *E. coli* transformed with pET28a⁺-ECD and pET28a⁺-ΔNT&LRR1 were treated with 0.5 mM isopropyl β-D-1-thiogalactopyranoside (IPTG) for 3 h at 25 °C; the cell pellets were then lysed in lysis buffer (50 mM NaH₂PO₄, 300 mM NaCl, 10 mM imidazole, pH 8.0) for 10 min on ice, treated with 1 mg/ml lysozyme (Beyotime, China, ST206), and processed through multiple freeze-thaw cycles in liquid nitrogen. The lysate was then sonicated, centrifuged, and subjected to Ni-NTA purification. The beads were washed with wash buffer (50 mM NaH₂PO₄, 300 mM NaCl, 20 mM imidazole, pH 8.0) four times, and eluted with elution buffer (50 mM NaH₂PO₄, 300 mM NaCl, 250 mM imidazole, pH 8.0). For expression of NT-LRR14 and NT-LRR8 protein, cDNAs of human LGR4 NT-LRR14 (28–396 aa) and LGR4 NT-LRR8 (28–249 aa) were subcloned into the pcDNA4T0 vector at the BamHI and EcoRI restriction sites with the CD8 sequence as a signal peptide. pcDNA4T0-NT-LRR14 and pcDNA4T0-NT-LRR8 were transfected and expressed in HEK293T cells. His-tagged NT-LRR14 and NT-LRR8 proteins were purified from HEK293T cell culture medium with the Ni-NTA system.

Surface plasmon resonance. SPR was determined using a Biacore X-100 plus instrument (GE). RANKL peptides were immobilized on the sensor chip (CM5) using the amine-coupling method according to standard protocols. RANKL peptide was diluted to 5 µg/ml in 10 mM sodium acetate buffer, pH 5.5. Immobilization was performed according to the manufacturer's recommendations. The kinetics and affinity assay were examined at 25 °C at a flow rate of 30 µl/min using PBS buffer. Diluted ECD peptides, NT-LRR14 peptides, NT-LRR8 peptides and OPG-Fc peptides were kept at 0 °C and placed into the rack tray before injection. The K_D values were calculated with the kinetics and affinity analysis option of Biacore X-100 plus evaluation software. Competition analysis was performed according to the software program "manual run". The LGR4-ECD and RANKL protein interaction was analyzed by regeneration with pH 2.0 Gly-HCl buffer, OPG-Fc protein was loaded as analyte to make sure

that the sensor chip was fully intact, and then LGR4-ECD protein was reloaded to compete with the OPG-RANKL interaction.

Docking and molecular modeling. We extracted single-chain truncated structures of RANKL and LGR4 from proteins *11QA* and *4KT1* (PDB ID), respectively. The crystal water in these proteins was removed in the extraction process. The 82–411 aa region of LGR4-ECD and the 161–316 aa region of RANKL were selected as candidate interfaces, and a truncation of RANKL (161–316 aa) and LGR4-ECD (25–528 aa) were docked into a complex with ZDock v3.0.2 software³⁸. The top ten complex models were selected as candidates. We selected the highest-confidence model from the ten candidate complexes using METopogram (Institute of Biophysics, Chinese Academy of Sciences, Beijing, China)³⁹. The complex model of RANKL-LGR4-ECD was shown by PyMol.

Immunofluorescence. For immunofluorescence, HEK293T cells were seeded in a 24-well plate on 0.1% gelatin-treated glass coverslips. All of the cells were transfected with siRNA for RANK (5'-CCAGAAGUAUGUGCUACCAU-3', 5'-UGGGUAGCACAUUCUUCUGGUU-3'). Each well was transfected with 0.5 µg of empty vector, human *LGR4*, or mouse *Rank* plasmid, respectively. Cells were subsequently incubated with either RANKL or RSPO1 at 37 °C for 20 min. After being washed twice with PBS, the cells were fixed in 4% paraformaldehyde, and incubated with anti-RANKL (IMGENEX, IMG-185A, 1:50) or anti-His antibody (Abmart, M30111, 1:1000) at 37 °C for 1 h. The images were obtained by laser-scanning confocal microscopy (Leica).

Flow-cytometric analysis. HEK293T cells were transfected with control siRNA or LGR4 siRNA and vector or LGR4 plasmids, incubated with 500 ng/ml of recombinant RANKL at 37 °C for 45 min, and then fixed with 4% paraformaldehyde. Cells were then incubated with 1 µg RANKL antibodies (IMGENEX, IMG-185A) or mouse IgG at 4 °C for 1 h. After washing, the cells were incubated with Alexa Fluor 488-labeled goat anti-mouse IgG (Invitrogen, a11001, 1:1,000) at 4 °C for 1 h, and then subjected to fluorescence-activated cell sorting (FACS) analysis (FACS caliber, BD) after washing.

Reporter-gene assay. To identify the possible G proteins that RANKL may activate, we used a luciferase reporter-gene system, as previously reported⁴⁰. The experiments were conducted in triplicate. Briefly, HEK293T cells were co-transfected with vector, luciferase and rennilla or *LGR4*, luciferase and rennilla plasmids as indicated. After seeding into 24-well plates, in some experiments, the cells were transfected with siRNA for RANK⁴¹ (5'-CCA GAAGUAUGUGCUACCAU-3', 5'-UGGGUAGCACAUUCUUCUGG UU-3') or siRNA for LGR4 (ref. 17) (5'-GAAAGUAAACUGUGUCAAUU-3', 5'-UUGACCACAGUUUACUUUCUU-3') by Lipofectamine 2000 (Invitrogen, 11668019). Then, cells were serum-starved with 1% FBS for 4 h, and incubated with indicated stimulators for 24 h. The luciferase assay was performed according to the manufacturer's protocol (Promega, E1960). To examine the bioactivity of LGR4-ECD protein, we used the TOP-FLASH system, as previously reported¹⁵. Briefly, 50 ng/ml RSPO1 and LGR4-ECD protein at the indicated concentrations were incubated for 12 h at 4 °C in DMEM culture containing 1% FBS. HEK293T cells were co-transfected with TOP-FLASH and rennilla or FOP-FLASH and rennilla plasmids. After seeding into 24-well plates, cells were stimulated with the RSPO1-LGR4-ECD mixture as indicated for 24 h. The luciferase assay was performed according to the manufacturer's protocol (Promega, E1960).

Enzyme-linked immunosorbent assay (ELISA). For cAMP ELISA, HEK293T cells were transfected with vector or LGR4 plasmids for 24 h. Cells were then pretreated with 250 nM 3-isobutyl-1-methylxanthine (IBMX) for 30 min, and incubated with RANKL at the indicated concentration for 24 h. cAMP production was examined according to the manufacturer's protocol (R&D, KGE002B) with samples pretreated at 95 °C for 15 s. For TRAP5b, PINP and osteocalcin ELISA, 8-week-old mice were euthanized for serum collection. Serum samples were then sent to USCN Life Science, Inc. (Wuhan, China) for analysis.

Calcium imaging and FLIPR calcium assay. We performed calcium imaging for the detection of intracellular calcium release, as previously described⁴².

For transient calcium mobilization, HEK293T cells were transiently transfected with plasmids using the calcium-phosphate method and following the standard protocol. 24 h after transfection, cells were loaded with 2 μ M fura-2AM (Molecular Probes, F1221). The basal 340/380 fluorescence signal of the cells in the field of view was monitored for 30 s, and then the cells were stimulated with 100 ng/ml or 200 ng/ml RANKL. After waiting for 20 s, transient calcium release was detected and imaged by LAMBDA DG-4 (Novato, CA, USA). For the RSP01 competition assay, HEK293T cells were transiently transfected with *Rank* siRNA (5'-CCAGAAGAUUGUGCUACCCAUU-3', 5'-UGGGUAGCACAUUCUUCUGGUU-3') using Lipofectamine 2000 (Invitrogen, 11668019), and with *LGR4* plasmid using the calcium-phosphate method and following the standard protocol. 24 h after transfection, cells were pretreated with RSP01 at 50 ng/ml, 100 ng/ml and 200 ng/ml, respectively, for 12 h. Cells were then loaded with 2 μ M fura-2AM (Molecular Probes, F1221). The basal 340/380 fluorescence signal of the cells in the field of view was monitored for 30 s, and then the cells were stimulated with 200 ng/ml RANKL. After waiting for 20s, transient calcium release was detected and imaged by LAMBDA DG-4 (Novato, CA, USA). To examine the calcium response, we performed a FLIPR calcium assay. Briefly, HEK293T cells were transiently transfected with plasmids using the calcium phosphate method and following the standard protocol. 24 h after transfection, cells were seeded in a 96-well plate at 8×10^4 cells per well, and then cultured with DMEM containing 10% FBS and 2 mM CaCl_2 for 12 h. Cells were washed with Hank's balanced salt solution (HBSS) containing 20 mM 4-(2-hydroxyethyl)-1-piperazineethanesulfonic acid (HEPES) and loaded with calcium-indicator dye from the FLIPR Calcium 5 Assay Kit (Molecular Devices, Sunnyvale, CA, USA), and incubated for 60 min at 37 °C. Measurements were performed via a FlexStation3 (Molecular Devices) set at 26 °C. Calcium signals (excitation at 485 nm and emission at 525 nm) were recorded for 2 min at 1.52 s intervals. The response of each well was calculated as ((maximum fluorescence value) – (minimum fluorescence value))/ minimum fluorescence value.

RT-qPCR analysis. For RT-qPCR analysis, total cellular RNA was extracted from cells using TRIzol reagent (Takara, 9109). PCR primers for *Nfact1*, Rous sarcoma oncogene (*Src*, also called *c-Src*), *cathepsin K*, *Trap*, calcitonin receptor (*Calcr*, also called *Ctr*) *Ctr*, *Rank*, *Gapdh*, *Fshr*, *Lhgr*, *Tshr*, *Lgr4*, *Lgr5*, *Lgr6*, relaxin/insulin-like family peptide receptor 1 (*Rxfp1*, also called *Lgr7*) and *Rxfp2* (also called *Lgr8*) are provided in **Supplementary Table 2**.

β -galactosidase (LacZ) and TRAP double staining. 10-day-old *Lgr4*^{+/-} mice were euthanized for femur bone isolation. The bones were washed with ice-cold LacZ fixation buffer (2% formaldehyde, 0.2% glutaraldehyde, 0.02% Nonidet P-40 in PBS) and incubated 2 h at 4 °C on a shaking platform. Fixed bones were then washed in LacZ washing buffer (2 mM MgCl_2 , 0.01% deoxycholate, 0.02% Nonidet P-40 in PBS, pH 8.0) twice (20 min each time). After being incubated in LacZ staining buffer (5 mM potassium hexacyanoferrate(III), 5 mM potassium hexacyanoferrate(II) trihydrate, 1 mg/ml X-gal in LacZ wash buffer) for 36 h at room temperature, the bone underwent decalcification with 0.5 M EDTA for 1 d followed by paraffin embedding, histological sectioning and TRAP staining. The same slides were captured before and after TRAP staining. The LacZ-TRAP double-staining regions were used for analysis.

Chromatin immunoprecipitation assay. RAW264.7 cells were treated with or without 20 ng/ml RANKL for 24 h, followed by ChIP analysis as previously reported¹², with only minor modifications. Briefly, cells were sonicated on ice with six cycles of Biorupter (Diagenode). The supernatant was incubated with 2 μ g IgG or NFATC1 antibody (Santa Cruz, sc-7294) at 4 °C for 4 h. Genomic DNA in immune complexes was extracted and prepared for PCR reactions. The primer sequences are provided in **Supplementary Table 2**.

Cell culture. For osteoclast differentiation analyses *in vitro*, we isolated bone marrow monocytes (BMMs) from 6-week-old WT and *Lgr4*^{-/-} or *Lgr4* CKO mouse femur and tibia bones, as previously described⁴⁰. The differentiation experiments were conducted in triplicate. BMMs were seeded into 24-well plates at a concentration of 1.5×10^4 cells per well. Cells were stimulated with 100 ng/ml RANKL (R&D, 462-TEC) and 10 ng/ml M-CSF (R&D, 416-ML) for

6 d, or for 8 d to assess osteoclast survival. Osteoclasts were fixed and stained using the TRAP staining kit (Sigma-Aldrich, 387A-1KT). For the osteoclast-survival assay, osteoclast ghosts were quantitated as dead osteoclasts. RAW264.7 cells were transfected with *Lgr4* siRNA (5'-GCAUCUUAACAAUAAATT-3', 5'-UUUAUGUUAUGAAGAUGCAG-3') or human *LGR4* plasmids using EugeneHD transfection reagent, as previously reported⁴⁰. Cells were then treated with RANKL for 3.5 d. For the pit-formation assay, mature osteoclasts were isolated, as previously described⁴⁰. Pits ($n = 50$) were stained with toluidine blue, and pit perimeter, area and depth were examined by laser-scanning confocal microscopy, as previously described⁴³. To assay osteoclast apoptosis, we performed TUNEL staining. Briefly, after RAW264.7 cells were transfected with siRNA using EugeneHD transfection reagent according to the manufacturer's instructions, the cells were seeded into 96-well plates and stimulated with 20 ng/ml RANKL for 3 d. TUNEL (Promega, G7130) staining was performed according to manufacturer's instructions. RAW264.7 and HEK293T cells were purchased from the Chinese Academy of Sciences Committee Type Culture Collection Cell Bank. The cell lines were authenticated and mycoplasma-tested by the Chinese Academy of Sciences Committee Type Culture Collection Cell Bank using PCR analysis.

Nuclear and cytoplasm extraction. RAW264.7 cells were transfected with $\text{G}\alpha_q^{\text{CA}}$ using Eugene HD (Roche Applied Science, 04709705001), and stimulated with 20 ng/ml RANKL for indicated times. Cells were then washed with cold PBS and resuspended in cell lysis buffer for 15 min, 3% NP-40 was added with vortexing. Samples were then rapidly centrifuged for 1 min at 14,000 rpm at 4 °C. The supernatant was the cytoplasm extract (CE), and the pellet was the nuclear extract (NE). Both the CE and NE were lysed with SDS-loading buffer and subjected to western blot using specific antibodies for NFATC1 (Santa Cruz, Sc-7294, 1:1,000), Actin (Sigma-Aldrich, A5441, 1:5,000), Histone3 (Cell Signaling Technologies, 9715L, 1:1,000) and $\text{G}\alpha_q$ (Santa Cruz, Sc-393, 1:1,000).

Western blot. For NF- κ B signaling analysis, RAW264.7 cells were transfected with or without 0.1, 0.2 μ g *LGR4* plasmids in 24-well plates. After 48 h, cells were stimulated with 100 ng/ml RANKL for 20 min, lysed in 1 \times SDS loading buffer and subjected to western blot using specific antibodies for phospho-p65 (Cell Signaling Technologies, 3033, 1:1,000), p65 (Cell Signaling Technologies, 3034, 1:1,000), I κ B α (Cell Signaling Technologies, 4814, 1:1,000) and actin (Sigma-Aldrich, A5441, 1:5000). For *LGR4*- $\text{G}\alpha_q$ -GSK3- β signaling, HEK293T cells were transfected either with *LGR4*-Flag or $\text{G}\alpha_q^{\text{CA}}$ plasmid. Cells were then stimulated without or with 100 ng/ml RANKL for 5, 15 and 30 min, lysed in 1 \times SDS loading buffer and subjected to western blot using specific antibodies for phospho-GSK3- β (Cell Signaling Technologies, 9336, 1:1,000), GSK3- β (Cell Signaling Technologies, 9315, 1:1,000), Flag (Sigma-Aldrich, F7425, 1:5,000), $\text{G}\alpha_q$ (Santa Cruz, Sc-393, 1:1,000) and GAPDH (Abmart, M20006F, 1:5,000).

Primary cultures of human peripheral blood mononuclear cells (PBMC) and bone giant-cell tumor (GCTB) cells. The use of all patient-derived tumor specimens was approved by the Institutional Review Board and the research ethics committee of Shanghai Changzheng Hospital under reference of 2010/081, which appeared in the proceedings of the meeting of the Ethics Committee on 18 November 2010. Informed consent was obtained from all tissue donors. The GCTB cells were isolated from tumor samples derived from tumor resections in Shanghai Changzheng Hospital, which were cultured in 37 °C with 5% CO_2 . Human peripheral blood mononuclear cells (PBMCs) were isolated from healthy donors by Ficoll gradient centrifugation (provided by the Shanghai Blood Center). The culture medium consisted of α -MEM supplemented with 10% FBS (FBS). For osteoclastogenesis, 5×10^5 PBMCs were seeded in a 96-well plate with 20 ng/ml human CSF1 (Sino Biological, Inc, 11792-H08Y). After 36 h, cells were stimulated with 50 ng/ml human RANKL (R&D, 6449-TEC) and 20 ng/ml human CSF1 for 8–9 d. Medium was changed every 2 d. Osteoclasts were fixed and stained using the TRAP-staining kit (Sigma-Aldrich, 387A-1KT).

Mice. Generation of *Lgr4*^{-/-} mice was previously described^{12,13}. *Tnfrsf11b*^{-/-} mice (strain 129S1/Sv) were purchased from the Shanghai Research Center For

Model Organisms. *Rspo4*^{-/-} mice (strain FVB) were generated from the Animal Center of East China Normal University. The generation for *Lgr4*^{fl^{oxed}} mice (strain C57/BL/6) is described in **Supplementary Figure 5a**. *Rank*^{fl^{oxed}} mice (strain C57BL/6) were described in reference⁹. *LysM-Cre* mice (strain C57BL/6) were described in reference⁴⁴. Both male and female mice were used in all experiments, except only male mice were used for LGR4-ECD treatment experiments and only female mice for the ovariectomy model. All of the mice were randomly assigned to groups. Maintenance, use and treatment of all animals were in accordance with accepted standards of the Ethics Committee at ECNU.

Micro-CT analyses. 3D micro-CT analyses and osteoclast morphometric analyses were performed as previously described¹³. For micro-CT, we scanned the bone using *in vivo* X-ray microtomography (Skyscan 1076, Bruker microCT) at a pixel size of 18 μ m, and analyzed the results according to the manufacturer's instructions. Region-of-interest (ROI) was defined from 0.215 mm (12 image slices) to 1.72 mm (106 image slices), where the growth plate slice was defined as 0 mm. Contrast was defined from 68–255; 3D analysis, BMD and 3D models were analyzed using CTAn software (Bruker microCT). 3D models were adjusted in CTVol software (Bruker microCT). For osteoclast morphometric analyses, 8-week-old, 16-week-old, and 24-week-old mouse femur bones and calvaria bones were isolated and fixed in 4% formaldehyde for 24 h. After decalcification with 0.5 M EDTA for 1–2 weeks, histological sectioning and TRAP staining for osteoclasts was performed. Osteoclast numbers, osteoclast surface area and eroded surface area were assessed by the OsteoMeasure Analysis System (Osteometrics, Atlanta, GA, USA), according to standard criteria.

Treatment with recombinant LGR4-ECD protein *in vivo*. For animal studies *in vivo*, mice were randomized for weight. For the ovariectomy-induced bone loss model, we sham-operated or ovariectomized 3-month-old C57BL/6 mice to induce osteoporosis. Ovariectomized mice were randomly divided into two groups (vehicle (PBS) versus recombinant LGR4-ECD protein, $n = 8$ per group). To analyze the therapeutic effect of recombinant LGR4-ECD protein, we injected LGR4-ECD protein (1 mg/kg/day) or vehicle into the tail vein after waiting 1 month beyond surgery for peak bone loss. After 5 weeks of treatment, the femurs and the L3 lumbar were isolated for micro-CT or histomorphometric analysis. For the RANKL-injection bone-resorption mouse model, the control protein, LGR4-ECD protein, RANKL-control protein, or RANKL-LGR4-ECD protein were injected into the calvaria of 6-week-old C57BL/6 male mice ($n = 6$) every day for 2 weeks. The concentration of control protein, LGR4-ECD protein, and RANKL protein was 1 mg/kg. At 15 d after the first injection, the mice were euthanized, and calvaria were collected. Calvaria were fixed in 4% formaldehyde,

permeabilized by 0.1% Triton X-100 for 1 h, and stained for TRAP activity with a TRAP kit (Sigma-Aldrich, 387A-1KT). 3D micro-CT analyses were performed according to a standard protocol. BMD and bone volume were analyzed by CT-analysis software (CTAn, Bruker microCT, Kontich, Belgium) and images were reconstituted by CT-volume software (CTvol, skyscan, CTAn, Bruker microCT, Kontich, Belgium). Similarly, 5-month-old 129 male *Tnfrsf11b*^{-/-} mice ($n = 6$ per group) were injected with control protein and LGR4-ECD protein into the calvaria or tibia bone at a concentration of 1 mg/kg every day for 2 weeks. For the tibia bone assay, PBS was injected into the left leg, and LGR4-ECD protein was injected into the right leg in the same mouse ($n = 11$ per group). Investigators were not blinded with respect to which protein was injected.

Statistical analyses. Data are represented as mean \pm s.d. for absolute values, as indicated in the vertical axis legend of the figures. The statistical significance of differential findings between experiments and controls was calculated by Excel 2007 (Microsoft Corp., Redmond, WA) using the two-tailed homoscedastic Student's *t* test. Significance was considered to be $P < 0.05$. Results are representative examples of more than two independent experiments. Data distribution was previously tested with the Kolmogorov-Smirnov test. Animal-experiment sample size was selected on the basis of power calculations seeking 80% power to detect a difference of 50% between groups with $\alpha = 0.05$. No animals were excluded. Investigators were not blinded during animal experiments.

38. Pierce, B.G., Hourai, Y. & Weng, Z. Accelerating protein docking in ZDOCK using an advanced 3D convolution library. *PLoS One* **6**, e24657 (2011).
39. Dai, W. *et al.* Improvement in low-homology template-based modeling by employing a model evaluation method with focus on topology. *PLoS One* **9**, e89935 (2014).
40. Li, C. *et al.* Maslinic acid suppresses osteoclastogenesis and prevents ovariectomy-induced bone loss by regulating RANKL-mediated NF- κ B and MAPK signaling pathways. *J. Bone Miner. Res.* **26**, 644–656 (2011).
41. Chu, G.C. *et al.* RANK- and c-Met-mediated signal network promotes prostate cancer metastatic colonization. *Endocr. Relat. Cancer* **21**, 311–326 (2014).
42. Wu, X. *et al.* Caffeic acid 3,4-dihydroxy-phenethyl ester suppresses receptor activator of NF- κ B ligand-induced osteoclastogenesis and prevents ovariectomy-induced bone loss through inhibition of mitogen-activated protein kinase/activator protein 1 and Ca²⁺-nuclear factor of activated T-cells cytoplasmic 1 signaling pathways. *J. Bone Miner. Res.* **27**, 1298–1308 (2012).
43. McMichael, B.K., Meyer, S.M. & Lee, B.S. c-Src-mediated phosphorylation of thyroid hormone receptor-interacting protein 6 (TRIP6) promotes osteoclast sealing zone formation. *J. Biol. Chem.* **285**, 26641–26651 (2010).
44. Zhang, Z. *et al.* Ferroportin1 deficiency in mouse macrophages impairs iron homeostasis and inflammatory responses. *Blood* **118**, 1912–1922 (2011).